

Constitutive Equations in Finite Element Codes: The INTERATOM Model in ABAQUS

D.K. Anding¹

Abstract: The paper deals with the implementation of constitutive equations for isotropic viscoplastic material behaviour into modern Finite Element codes like ABAQUS. ABAQUS provides an user interface called UMAT (USER MATERIAL) for the definition of quite general material behaviour. The user can take advantage of the complete Finite Element code from ABAQUS and has to focus only on the solution of the constitutive equations. Key problems are accuracy and stability of this local solution procedure, which comes from the numerical stiffness of the governing equations (mostly first order ordinary differential equations). The numerical stiffness does not allow to use explicit integration methods for the governing equations (not even higher order methods); implicit integration methods have to be used instead. In this paper it is shown that in case of isotropic material behaviour the local solution procedure for the governing equations is reduced to the solution of a single (generally nonlinear) scalar equation which can be solved efficiently by means of Newtons method.

keyword: Constitutive Equations, Viscoplasticity, Finite Elements, ABAQUS.

Nomenclature

c	hardening function
$\underline{\underline{C}}$	elasticity matrix
E	Young's modulus
E_t	tangent modulus
F	yield condition
g	hardening function
$\underline{\underline{I}}$	unity matrix
$\underline{\underline{J}}$	Jacobian matrix
\underline{n}	direction of plastic flow
t	time
T	temperature
Δ	increment
$\Delta \underline{\underline{\epsilon}}$	strain increment

$\Delta \underline{\underline{\epsilon}}_i$	inelastic strain increment
$\Delta \underline{\underline{\sigma}}$	stress increment
$\Delta \underline{\underline{\sigma}}_e$	elastic stress increment
Δt	time increment
$\underline{\underline{\epsilon}}$	strain tensor
$\dot{\underline{\underline{\epsilon}}}$	strain rate
$\dot{\underline{\underline{\epsilon}}}_e$	elastic strain rate
$\dot{\underline{\underline{\epsilon}}}_i$	inelastic strain rate
Φ	plastic multiplier
κ	isotropic hardening
$\dot{\kappa}$	isotropic hardening rate
Λ	overstress
ν	Poisson's ratio
$\underline{\underline{\sigma}}$	stress
$\underline{\underline{\sigma}}'$	stress tensor
$\underline{\underline{\sigma}}'$	deviatoric stress tensor
$\dot{\underline{\underline{\sigma}}}$	stress rate
ξ	kinematic hardening
$\underline{\underline{\xi}}$	kinematic hardening tensor
$\dot{\underline{\underline{\xi}}}$	kinematic hardening rate

1 Introduction

In commercial Finite Element codes like ABAQUS several well established models are available to describe the behaviour of a broad spectrum of materials, see ABAQUS (2003). Nevertheless, to describe the behaviour of special materials like those used in Aero Engines (AEs) or Industrial Gas Turbines (IGTs) more complex models are needed. For example Turbine blades and vanes made of Nickel base alloys are either conventionally casted (CC), directionally solidified (DS) or casted as single crystals (SX). CC materials show isotropic material behaviour in both the elastic and the inelastic range, whereas DS and SX materials are anisotropic in both ranges. Turbine blades and vanes made of these materials are exposed to severe thermomechanical loading, creep loads during holdtimes, vibrations and an oxidizing environment. This leads to High Cycle Fatigue (HCF) and

¹ MTU Aero Engines GmbH, Dachauer Straße 665, 80995 Munich, Germany.

Low Cycle Fatigue (LCF) as well as Thermo-Mechanical Fatigue (TMF) coupled with creep and material degradation from oxidation. Predicting the material behaviour of Nickel base alloys under these loads requires models which at least can describe cyclic plasticity coupled with creep, i. e. viscoplastic material models. For this purpose a number of models have been developed in the past, see Chaboche and Lemaitre (1990) and Meric and Cailletaud (1991), others are object of current research (especially for SX materials). For isotropic metallic materials (i. e. CC materials) in the high temperature range there are several models available to describe the viscoplastic material response, see e.g. Bruhns (1984). One of those models is the so called INTERATOM model. It is capable of describing isotropic and kinematic hardening coupled with time dependent effects like creep and relaxation.

However viscoplastic models like the INTERATOM model or the model of Chaboche are currently not available in ABAQUS. Therefore in this paper it is shown how viscoplastic isotropic material models can be implemented into ABAQUS. ABAQUS provides the user with a quite general interface called UMAT (USER MATERIAL), see ABAQUS (2003). The user has to provide in each increment the inelastic strain increment and the (consistent) tangential stiffness matrix to allow ABAQUS to build up the global stiffness matrix of the structure. To solve the first task, the Radial Return method, see Simo and Hughes (1998), is quite generally accepted to be most successful. To use the method a stable and accurate time integration scheme for the constitutive equations is needed, see e.g. Bruhns and Anding (1999). The procedure is described in detail in section 3. In section 4 three examples are shown. The first one is a simple LCF test with one element, the second one is a clamped bar under pure thermal load and the third one is a complex model of a turbine vane cluster under TMF loads. These examples prove the quality of the method. Special attention is paid to the CPU time needed for viscoplastic calculations with large models.

2 The INTERATOM model

The INTERATOM model is based on the assumption that the material behaviour up to a certain limit is purely elastic, and only beyond this limit shows rate-dependent effects like creep and relaxation. For the description of this inelastic behaviour the concept of overstresses, first pro-

posed by Perzyna, has been introduced in Bruhns (1984) together with an underlying rate-independent theory of elastic-plastic processes.

The basic idea of the model is to split the rate of deformation tensor into a reversible (elastic) and an irreversible part, which contains both rate-dependent and rate-independent effects

$$\dot{\boldsymbol{\varepsilon}} = \dot{\boldsymbol{\varepsilon}}_e + \dot{\boldsymbol{\varepsilon}}_i \quad (1)$$

In the present paper all material functions were determined from uniaxial static tests. Therefore the governing equations will be specialized to this case. For elastic-plastic material behaviour the INTERATOM model has the simple form

$$\begin{aligned} \dot{\boldsymbol{\sigma}} &= E_t(\kappa) \dot{\boldsymbol{\varepsilon}}, \\ \dot{\boldsymbol{\xi}} &= c(\kappa) \left(1 - \frac{E_t(\kappa)}{E}\right) \dot{\boldsymbol{\varepsilon}}, \\ \dot{\kappa} &= \sqrt{\frac{3}{2}} g(\kappa) \left(1 - \frac{E_t(\kappa)}{E}\right) |\dot{\boldsymbol{\varepsilon}}| \end{aligned} \quad (2)$$

with the tangent modulus $E_t(\kappa)$ and the two hardening functions $c(\kappa)$ and $g(\kappa)$, see Bruhns and Anding (1999).

For a description of rate-dependent effects like creep and relaxation the concept of overstresses is used. Introducing again the uniaxial form of the model with the so-called generalized overstress Λ , see Bruhns (1984), leads to the following constitutive equations

$$\begin{aligned} \dot{\boldsymbol{\sigma}} &= E \left(\dot{\boldsymbol{\varepsilon}} - \sqrt{\frac{2}{3}} \Phi(\Lambda, T) \right) \\ \dot{\boldsymbol{\xi}} &= c(\kappa, T) \sqrt{\frac{2}{3}} \Phi(\Lambda, T) \\ \dot{\kappa} &= \sqrt{\frac{3}{2}} g(\kappa, T) \sqrt{\frac{2}{3}} \Phi(\Lambda, T) \\ \Phi(\Lambda, T) &= 2\gamma(T) \frac{\Lambda}{E(T)} \left(1 + \frac{\Lambda}{c_4(T)}\right)^{c_5(T)} \\ \Lambda &= \sqrt{\left(\frac{2}{3} \boldsymbol{\sigma} - \boldsymbol{\xi}\right) \left(\boldsymbol{\sigma} - \frac{3}{2} \boldsymbol{\xi}\right) - \sqrt{g(\kappa, T)}} \end{aligned} \quad (3)$$

The INTERATOM model in the form given above contains 3 additional temperature dependent material parameters $\gamma(T)$, $c_4(T)$ and $c_5(T)$. These parameters can be identified from uniaxial creep tests or monotonic tensile tests with different strain rates, see Bruhns and Anding (1999).

3 Application of the radial return method to isotropic constitutive equations

Simo has shown in Simo and Hughes (1998) how the Radial Return method can be applied to quite general isotropic constitutive equations. The basic idea of the method is to perform first an *elastic predictor* step which determines definitely the current state of the material. Furthermore, with the elastic predictor the direction of plastic flow is given in case the current state of the material is beyond the yield surface.

If one uses the UMAT interface in ABAQUS, see ABAQUS (2003), to define isotropic viscoplastic material behaviour the following steps have to be performed:

From the global Newton-Raphson iteration both the time increment Δt and the strain increment $\Delta \underline{\underline{\epsilon}}$ are given. The stress increment $\Delta \underline{\underline{\sigma}}$ is calculated from the strain increment and the inelastic strain increment

$$\begin{aligned} \Delta \underline{\underline{\sigma}} &= \underline{\underline{C}} : (\Delta \underline{\underline{\epsilon}} - \Delta \underline{\underline{\epsilon}}_i) \\ {}^{t+\Delta t} \underline{\underline{\sigma}} &= {}^t \underline{\underline{\sigma}} + \Delta \underline{\underline{\sigma}} \end{aligned} \quad (4)$$

In Eq. 4 $\underline{\underline{C}}$ defines the elasticity matrix of the material. For isotropic material behaviour it is given in Appendix A. The users task is now to calculate the inelastic strain increment $\Delta \underline{\underline{\epsilon}}_i$ in each step. This calculation will be performed in every Gauss point of the Finite Element structure, therefore it has to take a reasonable time.

The assumption of the elastic predictor is $\Delta \underline{\underline{\epsilon}}_i = 0$. From Eq. 4 follows

$$\begin{aligned} \Delta \underline{\underline{\sigma}}_e &= \underline{\underline{C}} : \Delta \underline{\underline{\epsilon}} \\ {}^{t+\Delta t} \underline{\underline{\sigma}}_e &= {}^t \underline{\underline{\sigma}} + \Delta \underline{\underline{\sigma}}_e \end{aligned} \quad (5)$$

Here the elastic trial state ${}^{t+\Delta t} \underline{\underline{\sigma}}^{trial}$ is denoted with ${}^{t+\Delta t} \underline{\underline{\sigma}}_e$. The assumption $\Delta \underline{\underline{\epsilon}}_i = 0$ has to be checked. To do so it is necessary to calculate the deviatoric part of the elastic trial state

$${}^{t+\Delta t} \underline{\underline{\sigma}}'_e = {}^{t+\Delta t} \underline{\underline{\sigma}}_e - \frac{1}{3} \cdot tr({}^{t+\Delta t} \underline{\underline{\sigma}}_e) \cdot \underline{\underline{I}} \quad (6)$$

where $tr(\underline{\underline{\sigma}})$ denotes the first invariant of the stress tensor of three times the hydrostatic stress. With the deviatoric stress Eq. 6 the yield condition is checked

$$F = ({}^{t+\Delta t} \underline{\underline{\sigma}}'_e - {}^t \underline{\underline{\xi}}) : ({}^{t+\Delta t} \underline{\underline{\sigma}}'_e - {}^t \underline{\underline{\xi}}) - g({}^t \underline{\underline{\kappa}}) \quad (7)$$

In case that $F \leq 0$, the assumption $\Delta \underline{\underline{\epsilon}}_i = 0$ holds. Then the current stress state ${}^{t+\Delta t} \underline{\underline{\sigma}}$ is equal to ${}^{t+\Delta t} \underline{\underline{\sigma}}_e$. Therefore

the current state of the internal variables is

$$\begin{aligned} {}^{t+\Delta t} \underline{\underline{\xi}} &= {}^t \underline{\underline{\xi}}, \\ {}^{t+\Delta t} \underline{\underline{\kappa}} &= {}^t \underline{\underline{\kappa}}, \end{aligned} \quad (8)$$

and one can finish the time step. If $F > 0$, the assumption $\Delta \underline{\underline{\epsilon}}_i = 0$ cannot be true, i.e. the step cannot be elastic. This implies $\Delta \underline{\underline{\epsilon}}_i \neq 0$ and the elastic trial stress state has to be corrected.

The advantage of the Radial Return method is twofold; on the one hand one can use the previously calculated trial stress state Eq. 5 to find the final stress state, on the other hand the direction of plastic flow is definitely determined with the trial stress state:

The inelastic strain rate contains the so called plastic multiplier $\Phi(\Lambda, T)$ and the direction of plastic flow, namely the normal ${}^{t+\Delta t} \underline{\underline{n}}$ to the yield surface. This normal follows from the deviator of the trial stress state Eq. 6

$${}^{t+\Delta t} \underline{\underline{n}} = \frac{{}^{t+\Delta t} \underline{\underline{\sigma}}'_e - {}^t \underline{\underline{\xi}}}{\sqrt{({}^{t+\Delta t} \underline{\underline{\sigma}}'_e - {}^t \underline{\underline{\xi}}) : ({}^{t+\Delta t} \underline{\underline{\sigma}}'_e - {}^t \underline{\underline{\xi}})}}. \quad (9)$$

With Eq. 9 the only unknown to calculate the inelastic strain rate is the plastic multiplier $\Phi(\Lambda, T)$, which reduces the three dimensional problem to the determination of a scalar value. If $\Delta \underline{\underline{\epsilon}}_i \neq 0$ holds, then from Eq. 4 and Eq. 5 follows

$${}^{t+\Delta t} \underline{\underline{\sigma}} = {}^{t+\Delta t} \underline{\underline{\sigma}}_e - \underline{\underline{C}} : \Delta \underline{\underline{\epsilon}}_i \quad (10)$$

and the final stress state ${}^{t+\Delta t} \underline{\underline{\sigma}}$ is solely determined by the elastic trial stress state and the unknown plastic multiplier. This reduces the whole problem to the determination of the plastic multiplier $\Phi(\Lambda, T)$, as stated above.

Bathe, see Bathe (2002), and Simo, see Simo and Hughes (1998), have shown how a scalar equation (the so called effective stress function) for the plastic multiplier can be derived in case of an elasto-plastic material model. The root of this equation gives a value for the plastic multiplier. But also in case of a viscoplastic material model a single scalar equation for $\Phi(\Lambda, T)$ can be derived, as shown below.

First one has to choose a stable and accurate time integration scheme (for the definition of stability and accuracy see e.g. Bruhns and Anding (1999)). In the context of viscoplastic material models the midpoint rule is generally accepted to give reasonable results. The application

of the midpoint rule to the constitutive equations of the INTERATOM model leads to the following time discrete form of the model

$$\begin{aligned}\Delta \underline{\varepsilon}_i &= \frac{\Delta t}{2} \cdot \left({}^{t+\Delta t} \underline{\Phi} \cdot {}^{t+\Delta t} \underline{n} + {}^t \underline{\Phi} \cdot {}^t \underline{n} \right), \\ \Delta \underline{\xi} &= \frac{\Delta t}{2} \cdot \left({}^{t+\Delta t} c \cdot {}^{t+\Delta t} \underline{\Phi} \cdot {}^{t+\Delta t} \underline{n} + {}^t c \cdot {}^t \underline{\Phi} \cdot {}^t \underline{n} \right), \\ \Delta \kappa &= \frac{\Delta t}{2} \cdot \left(\sqrt{{}^{t+\Delta t} g} \cdot {}^{t+\Delta t} \underline{\Phi} + \sqrt{{}^t g} \cdot {}^t \underline{\Phi} \right). \end{aligned} \quad (11)$$

The updating of the internal variables of the model is done by

$$\begin{aligned}{}^{t+\Delta t} \underline{\xi} &= {}^t \underline{\xi} + \Delta \underline{\xi}, \\ {}^{t+\Delta t} \kappa &= {}^t \kappa + \Delta \kappa, \end{aligned} \quad (12)$$

respectively. To find the governing equation for the plastic multiplier the following steps have to be performed:

First the updated stress ${}^{t+\Delta t} \underline{\sigma}$ is expressed through Eq. 11. This leads to

$${}^{t+\Delta t} \underline{\sigma} = {}^{t+\Delta t} \underline{\sigma}_e - \underline{\underline{C}} : \left({}^{t+\Delta t} \underline{\Phi} \cdot {}^{t+\Delta t} \underline{n} + {}^t \underline{\Phi} \cdot {}^t \underline{n} \right) \cdot \frac{\Delta t}{2}. \quad (13)$$

Taking the deviatoric part of Eq. 13 leads to

$$\begin{aligned}{}^{t+\Delta t} \underline{\sigma}' &= {}^{t+\Delta t} \underline{\sigma}_e - \frac{1}{3} \cdot \text{tr} \left({}^{t+\Delta t} \underline{\sigma} \right) \cdot \underline{I} \\ &\quad - \underline{\underline{C}} : \left({}^{t+\Delta t} \underline{\Phi} \cdot {}^{t+\Delta t} \underline{n} + {}^t \underline{\Phi} \cdot {}^t \underline{n} \right) \cdot \frac{\Delta t}{2}. \end{aligned} \quad (14)$$

Taking into account that the trace of the deviator is Zero, the following equation for the *effective stress* is achieved

$$\begin{aligned}{}^{t+\Delta t} \underline{\sigma}' - {}^{t+\Delta t} \underline{\xi} &= {}^{t+\Delta t} \underline{\sigma}'_e - {}^t \underline{\xi} \\ &\quad + \frac{\Delta t}{2} \cdot \frac{1}{3} \text{tr} \left[\underline{\underline{C}} : \left({}^{t+\Delta t} \underline{\Phi} \cdot {}^{t+\Delta t} \underline{n} + {}^t \underline{\Phi} \cdot {}^t \underline{n} \right) \right] \cdot \underline{I} \\ &\quad - \underline{\underline{C}} : \left({}^{t+\Delta t} \underline{\Phi} \cdot {}^{t+\Delta t} \underline{n} + {}^t \underline{\Phi} \cdot {}^t \underline{n} \right) \cdot \frac{\Delta t}{2} \\ &\quad - \frac{\Delta t}{2} \cdot \left({}^{t+\Delta t} c \cdot {}^{t+\Delta t} \underline{\Phi} \cdot {}^{t+\Delta t} \underline{n} + {}^t c \cdot {}^t \underline{\Phi} \cdot {}^t \underline{n} \right). \end{aligned} \quad (15)$$

Taking the dot product of the effective stress with the normal ${}^{t+\Delta t} \underline{n}$ to the yield surface leads to

$$\begin{aligned} \left({}^{t+\Delta t} \underline{\sigma}' - {}^{t+\Delta t} \underline{\xi} \right) : {}^{t+\Delta t} \underline{n} &= \\ \sqrt{\left({}^{t+\Delta t} \underline{\sigma}' - {}^{t+\Delta t} \underline{\xi} \right) : \left({}^{t+\Delta t} \underline{\sigma}' - {}^{t+\Delta t} \underline{\xi} \right)}. \end{aligned} \quad (16)$$

From the definition Eq. 3 of the overstress follows that

$$\left({}^{t+\Delta t} \underline{\sigma}' - {}^{t+\Delta t} \underline{\xi} \right) : {}^{t+\Delta t} \underline{n} = {}^{t+\Delta t} \Lambda + \sqrt{{}^{t+\Delta t} g}. \quad (17)$$

This leads to a nonlinear scalar equation for the overstress ${}^{t+\Delta t} \Lambda$ and for the plastic multiplier ${}^{t+\Delta t} \Phi$, respectively. From Eq. 15, Eq. 16 and Eq. 17 follows

$$\begin{aligned} {}^{t+\Delta t} \Lambda &= \sqrt{\left({}^{t+\Delta t} \underline{\sigma}'_e - {}^t \underline{\xi} \right) : \left({}^{t+\Delta t} \underline{\sigma}'_e - {}^t \underline{\xi} \right)} - \sqrt{{}^{t+\Delta t} g} \\ &\quad - \frac{\Delta t}{2} \cdot {}^{t+\Delta t} \underline{\Phi} \cdot \left[\left(\underline{\underline{C}} : {}^{t+\Delta t} \underline{n} \right) : {}^{t+\Delta t} \underline{n} + {}^{t+\Delta t} c \right] \\ &\quad - \frac{\Delta t}{2} \cdot {}^t \underline{\Phi} \cdot \left[\left(\underline{\underline{C}} : {}^t \underline{n} \right) : {}^{t+\Delta t} \underline{n} + {}^t c \cdot {}^t \underline{n} : {}^{t+\Delta t} \underline{n} \right]. \end{aligned} \quad (18)$$

The steps shown above can be applied to almost every viscoplastic material model and will always reduce the system of ODEs (**O**rdinary **D**ifferential **E**quations) to a (generally nonlinear) scalar equation. Therefore the method is quite general.

3.1 Plastic material behaviour

The next task is the solution of Eq. 18 to find the overstress ${}^{t+\Delta t} \Lambda$. In the static case, the overstress ${}^{t+\Delta t} \Lambda \equiv 0$, therefore the problem is reduced to determine the isotropic hardening ${}^{t+\Delta t} \kappa$ by solving

$$\begin{aligned} f \left({}^{t+\Delta t} \kappa \right) &= \sqrt{\left({}^{t+\Delta t} \underline{\sigma}'_e - {}^t \underline{\xi} \right) : \left({}^{t+\Delta t} \underline{\sigma}'_e - {}^t \underline{\xi} \right)} - \sqrt{{}^{t+\Delta t} g} \\ &\quad - \frac{\Delta t}{2} \cdot {}^{t+\Delta t} \underline{\Phi} \cdot \left[\left(\underline{\underline{C}} : {}^{t+\Delta t} \underline{n} \right) : {}^{t+\Delta t} \underline{n} + {}^{t+\Delta t} c \right] \\ &\quad - \frac{\Delta t}{2} \cdot {}^t \underline{\Phi} \cdot \left[\left(\underline{\underline{C}} : {}^t \underline{n} \right) : {}^{t+\Delta t} \underline{n} + {}^t c \cdot {}^t \underline{n} : {}^{t+\Delta t} \underline{n} \right] \\ &= 0, \end{aligned} \quad (19)$$

with ${}^{t+\Delta t} \Phi$ from Eq. 11

$${}^{t+\Delta t} \Phi = \frac{{}^{t+\Delta t} \kappa - {}^t \kappa}{\frac{\Delta t}{2} \cdot \sqrt{{}^{t+\Delta t} g}} - {}^t \Phi \cdot \sqrt{\frac{{}^t g}{{}^{t+\Delta t} g}}. \quad (20)$$

For the solution of Eq. 19 Newton's method is applied

$${}^{t+\Delta t} \kappa_{i+1} = {}^{t+\Delta t} \kappa_i - \frac{f \left({}^{t+\Delta t} \kappa_i \right)}{f' \left({}^{t+\Delta t} \kappa_i \right)}; i = 0, 1, 2, \dots \quad (21)$$

with

$${}^{t+\Delta t} \kappa_0 = {}^t \kappa. \quad (22)$$

The derivative $f' \left({}^{t+\Delta t} \kappa \right)$ is given in Appendix B.

3.2 Viscoplastic material behaviour

In the viscoplastic case both overstress ${}^{t+\Delta t}\Lambda$ and isotropic hardening ${}^{t+\Delta t}\kappa$ are coupled, therefore the following two equations have to be solved simultaneously

$$\begin{aligned} f_1({}^{t+\Delta t}\kappa, {}^{t+\Delta t}\Lambda) &= {}^{t+\Delta t}\kappa - {}^t\kappa \\ &- \frac{\Delta t}{2} \cdot \left(\sqrt{{}^{t+\Delta t}g} \cdot {}^{t+\Delta t}\Phi + \sqrt{{}^tg} \cdot {}^t\Phi \right) \\ &= 0 \end{aligned} \quad (23)$$

and

$$\begin{aligned} f_2({}^{t+\Delta t}\kappa, {}^{t+\Delta t}\Lambda) &= \sqrt{({}^{t+\Delta t}\underline{\sigma}'_e - {}^t\underline{\xi}) : ({}^{t+\Delta t}\underline{\sigma}'_e - {}^t\underline{\xi})} \\ &- \sqrt{{}^{t+\Delta t}g} - \frac{\Delta t}{2} \cdot {}^{t+\Delta t}\Phi \cdot \left[\left(\underline{\underline{C}} : {}^{t+\Delta t}\underline{n} \right) : {}^{t+\Delta t}\underline{n} \right. \\ &+ \left. {}^{t+\Delta t}c \right] - \frac{\Delta t}{2} \cdot {}^t\Phi \cdot \left[\left(\underline{\underline{C}} : {}^t\underline{n} \right) : {}^{t+\Delta t}\underline{n} + {}^tc \cdot {}^t\underline{n} : {}^{t+\Delta t}\underline{n} \right] \\ &- {}^{t+\Delta t}\Lambda \\ &= 0, \end{aligned} \quad (24)$$

with ${}^{t+\Delta t}\Phi$ from Eq. 3

$${}^{t+\Delta t}\Phi = 2\gamma(T) \frac{{}^{t+\Delta t}\Lambda}{E(T)} \left(1 + \frac{{}^{t+\Delta t}\Lambda}{c_4(T)} \right)^{c_5(T)}. \quad (25)$$

For the solution of Eq. 23 and Eq. 24 Newton's method is applied. In the following the abbreviations

$$\vec{x} = \begin{pmatrix} x_1 \\ x_2 \end{pmatrix} = \begin{pmatrix} {}^{t+\Delta t}\kappa \\ {}^{t+\Delta t}\Lambda \end{pmatrix} \quad (26)$$

are used. First the search direction has to be determined by solving the linear equation system

$$\underline{J} \cdot \vec{s} = -\vec{f}(\vec{x}^k); k = 0, 1, 2, \dots \quad (27)$$

with the Jacobian

$$J_{ij} = \frac{\partial f_i(\vec{x}^k)}{\partial x_j}. \quad (28)$$

The solution of Eq. 27 is

$$\begin{aligned} s_1 &= \frac{J_{12} \cdot f_2 - J_{22} \cdot f_1}{J_{11} \cdot J_{22} - J_{12} \cdot J_{21}} \\ s_2 &= \frac{J_{21} \cdot f_1 - J_{11} \cdot f_2}{J_{11} \cdot J_{22} - J_{12} \cdot J_{21}} \end{aligned} \quad (29)$$

Next one has to perform the Newton step

$$\vec{x}^{k+1} = \vec{x}^k + \vec{s} \quad (30)$$

with the starting values

$$\vec{x}^0 = \begin{pmatrix} {}^t\kappa \\ {}^t\Lambda \end{pmatrix}. \quad (31)$$

The derivatives in the Jacobian Eq. 28 are given in Appendix C.

3.3 Tangential Stiffness Matrix

The last task in the implementation of inelastic material models into Finite Element codes is the calculation of the *tangential stiffness matrix*. The convergence of the global Newton-Raphson iteration, see Bathe (2002), is determined by the consistency of this matrix. Consistency in this context means that the formula for the tangential stiffness matrix is consistent with the underlying time integration scheme (here the midpoint rule). Only if this consistency holds the full convergence of the global iteration can be achieved. Otherwise the stepsize can become very small (or the solution does not converge at all).

For the midpoint rule given above the consistent tangential stiffness matrix is

$$\frac{\partial {}^{t+\Delta t}\underline{\sigma}}{\partial \Delta \underline{\epsilon}} = \frac{\Delta t}{2} \cdot \left(\frac{\partial {}^t\underline{\sigma}}{\partial \Delta \underline{\epsilon}} + \frac{\partial {}^{t+\Delta t}\underline{\sigma}}{\partial \Delta \underline{\epsilon}} \right). \quad (32)$$

From Eq. 4 follows

$$\frac{\partial {}^{t+\Delta t}\underline{\sigma}}{\partial \Delta \underline{\epsilon}} = \frac{\partial \Delta \underline{\sigma}}{\partial \Delta \underline{\epsilon}} = \frac{\partial \left[\underline{\underline{C}} : (\Delta \underline{\epsilon} - \Delta \underline{\epsilon}_i) \right]}{\partial \Delta \underline{\epsilon}}. \quad (33)$$

In case of elastic material behaviour, i.e. $\Delta \underline{\epsilon}_i = 0$, the tangential stiffness matrix is equal to the elasticity matrix Eq. 35 of the material

$$\frac{\partial {}^{t+\Delta t}\underline{\sigma}}{\partial \Delta \underline{\epsilon}} = \underline{\underline{C}}. \quad (34)$$

In case of inelastic material behaviour the tangential stiffness matrix Eq. 33 differs from the elasticity matrix; its main components are shown in Appendix D.

4 Examples

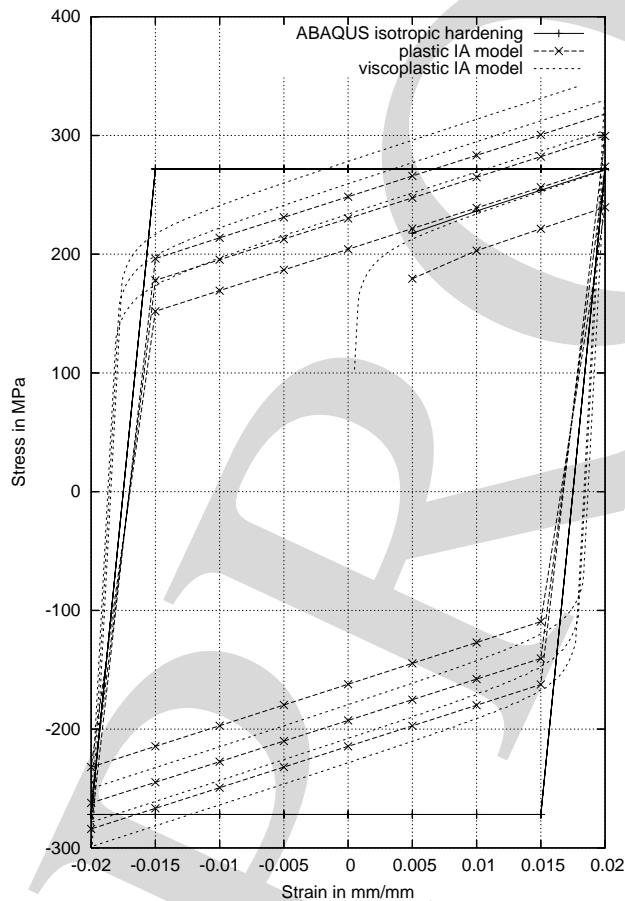
In this section three examples are presented to show how the implementation of the INTERATOM model based on the solution of the effective stress function in section 3 works in ABAQUS. These examples are summarized in Tab. 1.

Table 1 : Model size for the different examples

Example	No. of Nodes	No. of Elements
LCF – 1 element	8	1
bar under thermal load	1016	475
TMF – Turbine Vane Cluster	90981	66359

Table 2 : Comparison of CPU time between different material models for the first example

LCF – 1 element	ABAQUS isotropic hardening	plastic IA model	viscoplastic IA model
CPU time (sec)	1.93	2.39	4.95
Increments	52	52	99
Iterations	59	79	256

**Figure 1** : Prediction of a strain controlled LCF test with three different models

The first example is a strain controlled LCF test. This example is performed with one 8-noded hexahedral element for both the plastic and viscoplastic INTERATOM model. For comparison purposes (mainly for CPU time) the same calculation was done with the ABAQUS isotropic hardening model. As shown in Fig. 1 the ABAQUS isotropic hardening model cannot predict cyclic hardening behaviour, which is obvious, because it does not contain any parameters for cyclic behaviour (e. g. kinematic hardening), whereas both the plastic and viscoplastic INTERATOM model can predict cyclic hardening. Better results would be achieved with the ABAQUS kinematic hardening model or even better with the ABAQUS combined hardening model, but both models do not take into account creep and relaxation effects and their interaction with the cyclic behaviour (see example 3). Only the viscoplastic INTERATOM model is capable of doing so, because it also takes into account the strain rate influence, whereas the plastic INTERATOM model and the plastic ABAQUS models are independent of the strain rate.

In Tab. 2 the computational effort for the three different models is compared. What can be seen is that the ABAQUS isotropic hardening model is faster than the two others, but the CPU time does not differ much. Between the plastic INTERATOM model and ABAQUS isotropic hardening it is only a factor 1.24, which is very close to 1. Between the viscoplastic INTERATOM model and ABAQUS isotropic hardening it is a factor 2.57, which is reasonable if one takes into account the higher capability of the viscoplastic INTERATOM model.

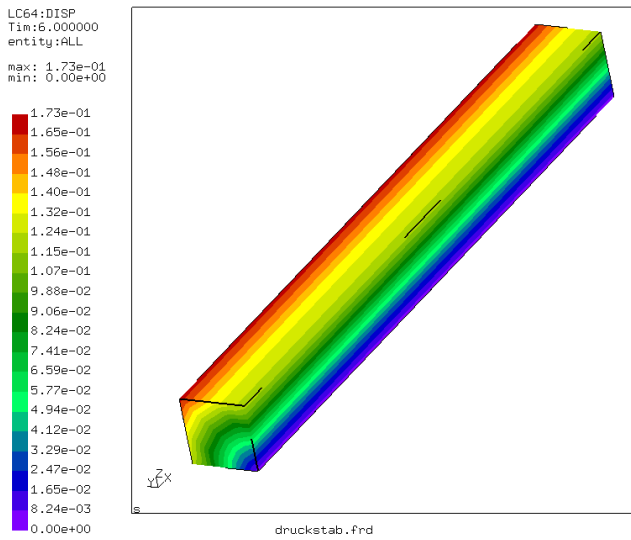


Figure 2 : Thermal expansion of a bar under thermal load (the figure shows the resultant displacement)

The second example is a bar under pure thermal load, which is clamped on both sides in such a way that thermal expansion perpendicular to the main axis (here the x-axis) is free. Therefore only compressive stresses in the direction of the main axis can occur. The dimension of the bar is $10 \times 10 \times 100$ mm.

Fig. 2 shows the thermal expansion of the bar.

The resultant compressive stress as a function of temperature can be seen in Fig. 3. The higher the temperature, the more yielding of the material occurs. As before the calculation was performed with all three different models, i. e. the ABAQUS isotropic hardening and the plastic and viscoplastic INTERATOM model. What can be seen is that all three models give similar results, which is obvious, because for this monotonic type of loading cyclic behaviour does not play a role. But this example is an important test for the third example, namely a Turbine Vane Cluster under TMF loading. Only if the thermal stresses in this simple test can be predicted correctly, TMF stresses in a complex structure can be predicted.

The comparison of the computational effort in Tab. 3 shows the same picture as before; again the ABAQUS isotropic hardening model is the fastest one. Both the plastic and viscoplastic INTERATOM model are slower, but again not much (factors 1.13 and 1.64, respectively).

The third example is a Turbine Vane Cluster under TMF

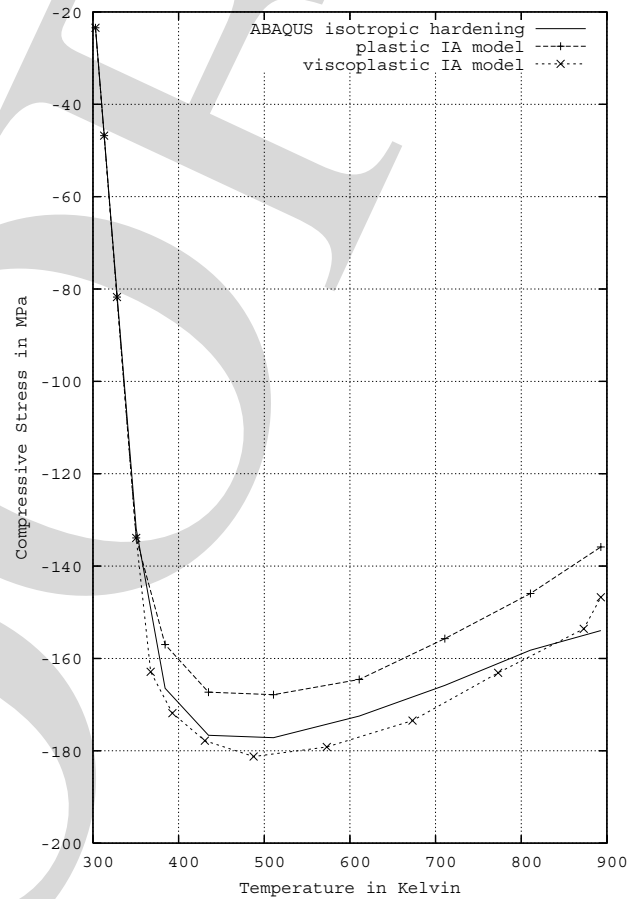


Figure 3 : Compressive stress as a function of temperature in a bar under thermal load

loading. This type of loading is the main purpose of viscoplastic models; to predict TMF life of a structure like this Turbine Vane or an Exhaust Manifold in car engines, these models are needed. With pure elastic models one cannot predict cyclic hardening effects, with pure plastic models one cannot predict creep effects during hold-times, especially at high temperatures. Fig. 4 shows a typical temperature distribution in a Turbine Vane Cluster during a TMF cycle.

The resultant stresses during a TMF cycle are very complex; they vary at each location with time and temperature, because the loading from thermal gradients and gas loads in a Turbine vary for each time step. The boundary conditions for this analysis are also quite complex; first the transient 3D temperature field for the entire TMF cycle is needed, second the transient 3D gas loads are needed for each time step, third thermal expansion has

Table 3 : Comparison of CPU time between different material models for the second example

bar under thermal load	ABAQUS isotropic hardening	plastic IA model	viscoplastic IA model
CPU time (sec)	5.81	6.58	9.51
Increments	11	11	13
Iterations	12	18	29

Table 4 : Comparison of CPU time between different material models for the third example

TMF – Turbine Vane Cluster	ABAQUS isotropic hardening	viscoplastic IA model
CPU time (sec)	4962.7	72864.0
Increments	29	230
Iterations	53	965

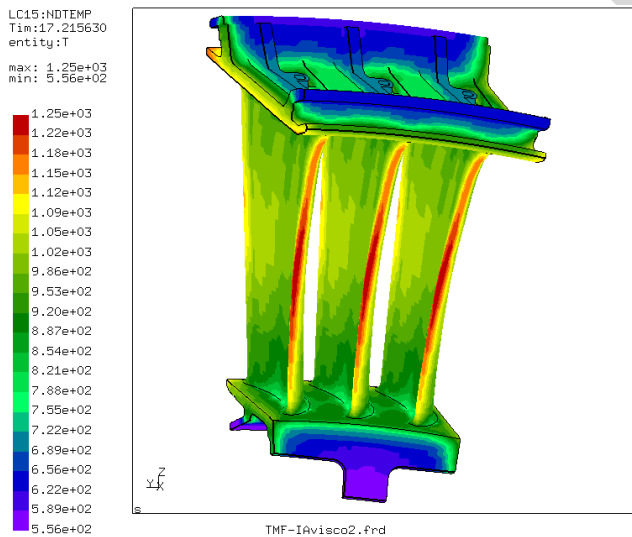


Figure 4 : Temperature distribution in a Turbine Vane Cluster for one time step of a TMF cycle

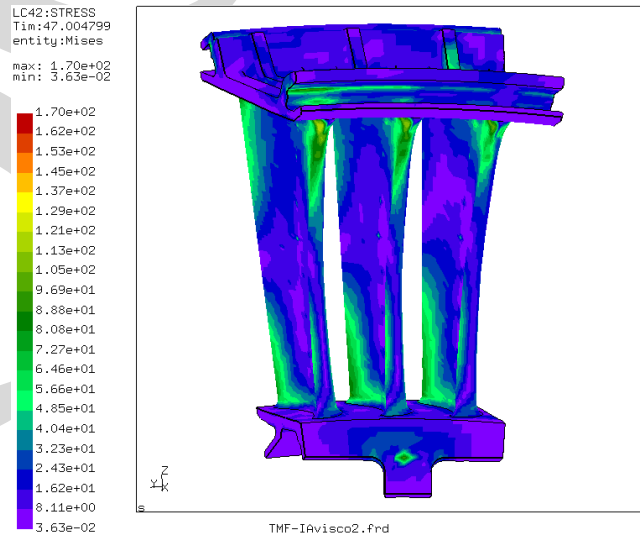


Figure 5 : Von Mises Stress distribution in a Turbine Vane Cluster for one time step of a TMF cycle

to be taken into account for the prediction of thermal stresses and displacement boundary conditions have to be defined in such a way that contact conditions between Vane Cluster and Turbine Case are realistic and that no additional stresses are introduced into the structure (one has to take into account that thermal stresses occur from both displacement boundary conditions and from thermal gradients). Fig. 5 shows the stress distribution in the Vane Cluster for one time step of the TMF cycle.

For a constant location in the Vane Cluster the TMF cycle can be plotted, e. g. as Stress over Temperature, this material response differs for each location of the Struc-

ture. Fig. 6 shows the TMF cycle for the outer diameter leading edge of the Vane Cluster.

What can be seen is that the simple ABAQUS isotropic hardening model gives a reasonable approximation of the first TMF cycle in the tensile range, but not in the compressive range, which is obvious, because it cannot predict the Bauschinger effect. Furthermore it cannot predict the cyclic hardening and the creep behaviour during hold times at high temperature. Again better results would be achieved with the ABAQUS kinematic hardening model or even better with the ABAQUS combined hardening model, but both models do not take into ac-

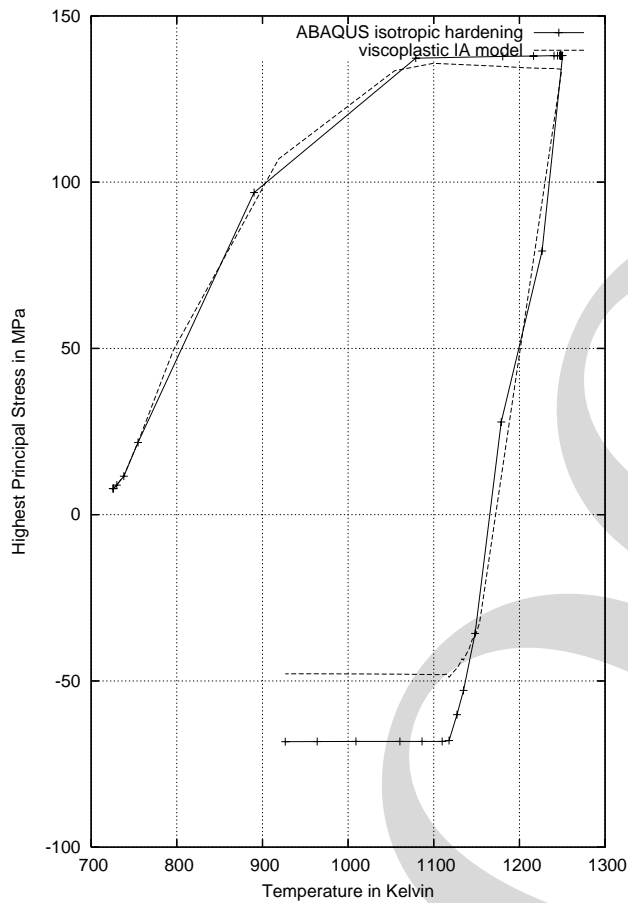


Figure 6 : TMF cycle at one location of the Vane Cluster

count creep and relaxation effects and their interaction with the cyclic behaviour. Only the viscoplastic INTERATOM model is capable of doing so. If one takes into account that life prediction methods based on stress or strain ranges are very sensitive to changes in the stress or strain range, it becomes clear that TMF life prediction based on the ABAQUS isotropic hardening model will be inaccurate, whereas the viscoplastic INTERATOM model will lead to better results.

Take for example a simple Woehler curve with the number of cycles to failure $N_f = \frac{1}{2} \cdot \left(\frac{\Delta\sigma}{1000}\right)^{-5}$. The ABAQUS isotropic hardening model in Fig. 6 predicts a stress range $\Delta\sigma$ of 205 MPa, which would give 1381 cycles to failure, whereas the INTERATOM model predicts a stress range $\Delta\sigma$ of 180 MPa, which would give 2646 cycles to failure. This means a difference of a factor 2 in life (imagine the consequences for the design of the Vane Cluster if the life requirement is e. g. 2500 TMF cycles).

The computational effort for both models is compared in Tab. 4.

From Tab. 4 it becomes clear that the computational effort for viscoplastic calculations with more complex models like this Vane Cluster is much higher than for simple plastic calculations, but one has to take into account the points stated above. For accurate TMF life predictions viscoplastic calculations are necessary. But the calculation time for the viscoplastic calculation is still reasonable (factor 14.7 against ABAQUS isotropic hardening).

5 Conclusions

A general method is presented how to implement constitutive equations for isotropic viscoplastic material behaviour into Finite Element codes like ABAQUS. The method consists of a local solution procedure of a nonlinear scalar equation for the plastic multiplier. For the solution of the nonlinear equation Newton's method is used.

For the description of viscoplastic material behaviour the so-called INTERATOM model is chosen. In this model the plastic multiplier is a function of the so-called over-stress. Furthermore the model is capable of describing isotropic and kinematic hardening coupled with creep and relaxation.

Three examples show the quality of the method. CPU time for viscoplastic calculations with the INTERATOM model in ABAQUS is low enough to allow cyclic calculations with large models.

We believe that the approach presented here is a general method for the implementation of various constitutive equations for isotropic viscoplastic material behaviour into Finite Element codes.

References

- ABAQUS (2003): *ABAQUS ANALYSIS USER'S MANUAL*. ABAQUS, Inc.
- Bathe, K.-J. (2002): *Finite-Elemente-Methoden*. Springer-Verlag Berlin Heidelberg New York.
- Bruhns, O. T. (1984): The INTERATOM (IA) Model. In: O. T. Bruhns (ed) *Constitutive Modelling in the Range of Inelastic Deformations - A State of the Arts Report*. Technical report, INTERATOM, 1984.

Bruhns, O. T.; Anding, D. K. (1999): On the simultaneous estimation of model parameters used in constitutive laws for inelastic material behaviour. *Int. J. Plasticity*, vol. 15, pp. 1311–1340.

Chaboche, J. L.; Lemaitre, J. (1990): *Mechanics of Solid Materials*. Cambridge University Press.

Meric, L.; Cailletaud, G. (1991): Single Crystal Modeling for Structural Calculations: Part 2 - Finite Element Implementation. *Journal of Engineering Materials and Technology*, vol. 113.

Simo, J. C.; Hughes, T. J. R. (1998): *Computational Inelasticity*. Springer Verlag New York, Inc.

Appendix B: Derivative of the nonlinear function for plastic material behaviour

The derivative of Eq. 19 with respect to the isotropic hardening κ is

$$f'({}^{t+\Delta t}\kappa) = -\frac{1}{2 \cdot \sqrt{{}^{t+\Delta t}g}} \cdot \frac{d^{t+\Delta t}g}{d\kappa} - \frac{\Delta t}{2} \cdot \left(\left[\frac{\sqrt{{}^{t+\Delta t}g} - \frac{{}^{t+\Delta t}\kappa - {}^t\kappa}{2 \cdot \sqrt{{}^{t+\Delta t}g}} \cdot \frac{d^{t+\Delta t}g}{d\kappa}}{\frac{\Delta t}{2} \cdot {}^{t+\Delta t}g} + \frac{{}^t\Phi}{2} \cdot \frac{\sqrt{{}^tg}}{({}^{t+\Delta t}g)^{\frac{3}{2}}} \cdot \frac{d^{t+\Delta t}g}{d\kappa} \right] \cdot \left[\underline{\underline{C}} : {}^{t+\Delta t}\underline{n} \right] : {}^{t+\Delta t}\underline{n} + {}^{t+\Delta t}c \right) + \left[\frac{{}^{t+\Delta t}\kappa - {}^t\kappa}{\frac{\Delta t}{2} \cdot \sqrt{{}^{t+\Delta t}g}} - {}^t\Phi \cdot \sqrt{\frac{{}^tg}{{}^{t+\Delta t}g}} \right] \cdot \frac{d^{t+\Delta t}c}{d\kappa}. \quad (36)$$

The derivatives of the material functions $g(\kappa)$ and $c(\kappa)$ with respect to κ are given in Bruhns and Anding (1999).

Appendix C: Derivatives of the nonlinear functions for viscoplastic material behaviour

The different components of the Jacobian Eq. 28 are

$$J_{11} = \frac{\partial f_1}{\partial {}^{t+\Delta t}\kappa} = 1 - \frac{\Delta t}{2} \cdot {}^{t+\Delta t}\Phi \cdot \frac{1}{2 \cdot \sqrt{{}^{t+\Delta t}g}} \cdot \frac{d^{t+\Delta t}g}{d\kappa}$$

$$J_{12} = \frac{\partial f_1}{\partial {}^{t+\Delta t}\Lambda} = -\frac{\Delta t}{2} \cdot \sqrt{{}^{t+\Delta t}g} \cdot \frac{d^{t+\Delta t}\Phi}{d^{t+\Delta t}\Lambda}$$

$$J_{21} = \frac{\partial f_2}{\partial {}^{t+\Delta t}\kappa} = -\frac{1}{2 \cdot \sqrt{{}^{t+\Delta t}g}} \cdot \frac{d^{t+\Delta t}g}{d\kappa} - \frac{\Delta t}{2} \cdot {}^{t+\Delta t}\Phi \cdot \frac{d^{t+\Delta t}c}{d\kappa}$$

$$J_{22} = \frac{\partial f_2}{\partial {}^{t+\Delta t}\Lambda} = -1 - \frac{d^{t+\Delta t}\Phi}{d^{t+\Delta t}\Lambda} \cdot \frac{\Delta t}{2} \cdot \left[\left(\underline{\underline{C}} : {}^{t+\Delta t}\underline{n} \right) : {}^{t+\Delta t}\underline{n} + {}^{t+\Delta t}c \right] \quad (37)$$

with the derivative of the plastic multiplier Eq. 25 with respect to the overstress Λ

$$\frac{d^{t+\Delta t}\Phi}{d^{t+\Delta t}\Lambda} = \frac{2\gamma}{E} \left(1 + \frac{{}^{t+\Delta t}\Lambda}{c_4} \right)^{c_5} \cdot \left[1 + \frac{{}^{t+\Delta t}\Lambda \cdot \frac{c_5}{c_4}}{1 + \frac{{}^{t+\Delta t}\Lambda}{c_4}} \right]. \quad (38)$$

Appendix A: Isotropic elasticity matrix

In Eq. 4 $\underline{\underline{C}}$ defines the elasticity matrix of the material. In the isotropic case $\underline{\underline{C}}$ is given as

$$\underline{\underline{C}} = \frac{E \cdot (1-\nu)}{(1+\nu) \cdot (1-2\nu)} \cdot \begin{pmatrix} 1 & \frac{\nu}{1-\nu} & \frac{\nu}{1-\nu} & 0 & 0 & 0 \\ \frac{\nu}{1-\nu} & 1 & \frac{\nu}{1-\nu} & 0 & 0 & 0 \\ \frac{\nu}{1-\nu} & \frac{\nu}{1-\nu} & 1 & 0 & 0 & 0 \\ 0 & 0 & 0 & \frac{1-2\nu}{1-\nu} & 0 & 0 \\ 0 & 0 & 0 & 0 & \frac{1-2\nu}{1-\nu} & 0 \\ 0 & 0 & 0 & 0 & 0 & \frac{1-2\nu}{1-\nu} \end{pmatrix} \quad (35)$$

with Young's modulus E and Poisson's ratio ν .

Appendix D: Tangential stiffness matrix

The main components of the tangential stiffness matrix are shown below. The other components are analogous (refer to Eq. 33).

$$\begin{aligned}
 \frac{\partial \Delta \sigma_{11}}{\partial \Delta \varepsilon_{11}} &= \frac{E \cdot (1 - \nu)}{(1 + \nu) \cdot (1 - 2\nu)} \left[1 - \frac{1 - 2\nu}{1 - \nu} \cdot \frac{(\sigma'_{11} - \xi_{11}) \cdot (\sigma'_{11} - \xi_{11})}{(\underline{\sigma}' - \underline{\xi}) : (\underline{\sigma}' - \underline{\xi}) \cdot \left(1 + \frac{2}{3} \cdot (1 + \nu) \cdot \frac{E_t(\kappa)}{E - E_t(\kappa)}\right)} \right] \\
 \frac{\partial \Delta \sigma_{11}}{\partial \Delta \varepsilon_{22}} &= \frac{E \cdot (1 - \nu)}{(1 + \nu) \cdot (1 - 2\nu)} \left[\frac{\nu}{1 - \nu} - \frac{1 - 2\nu}{1 - \nu} \cdot \frac{(\sigma'_{11} - \xi_{11}) \cdot (\sigma'_{22} - \xi_{22})}{(\underline{\sigma}' - \underline{\xi}) : (\underline{\sigma}' - \underline{\xi}) \cdot \left(1 + \frac{2}{3} \cdot (1 + \nu) \cdot \frac{E_t(\kappa)}{E - E_t(\kappa)}\right)} \right] \\
 \frac{\partial \Delta \sigma_{11}}{\partial \Delta \varepsilon_{12}} &= \frac{E \cdot (1 - \nu)}{(1 + \nu) \cdot (1 - 2\nu)} \left[-\frac{1 - 2\nu}{1 - \nu} \cdot \frac{2 \cdot (\sigma'_{11} - \xi_{11}) \cdot (\sigma'_{12} - \xi_{12})}{(\underline{\sigma}' - \underline{\xi}) : (\underline{\sigma}' - \underline{\xi}) \cdot \left(1 + \frac{2}{3} \cdot (1 + \nu) \cdot \frac{E_t(\kappa)}{E - E_t(\kappa)}\right)} \right] \\
 \frac{\partial \Delta \sigma_{12}}{\partial \Delta \varepsilon_{12}} &= \frac{E \cdot (1 - \nu)}{(1 + \nu) \cdot (1 - 2\nu)} \left[\frac{1 - 2\nu}{1 - \nu} - \frac{1 - 2\nu}{1 - \nu} \cdot \frac{2 \cdot (\sigma'_{12} - \xi_{12}) \cdot (\sigma'_{12} - \xi_{12})}{(\underline{\sigma}' - \underline{\xi}) : (\underline{\sigma}' - \underline{\xi}) \cdot \left(1 + \frac{2}{3} \cdot (1 + \nu) \cdot \frac{E_t(\kappa)}{E - E_t(\kappa)}\right)} \right] \quad (39)
 \end{aligned}$$

PROOF